Check for updates

ADVANCED CHARACTERIZATION AND TESTING OF IRRADIATED MATERIALS

Localized Helium Implantation in SiC_f/SiC_m Composites Comparing Fiber and Matrix Swelling

M.V. AMBAT, 1 D. FRAZER, 1,2 M.P. POPOVIC, 1 M. BALOOCH, 1 S. STEVENSON, 1 A. SCOTT, 1 J. KABEL, 1 and P. HOSEMANN $_{\hbox{\scriptsize 0}}^{1,3,4}$

1.—Department of Nuclear Engineering, University of California Berkeley, Berkeley, CA 94720–1730, USA. 2.—Materials Science and Technology Division, Los Alamos National Laboratory, Los Alamos, NM 87545, USA. 3.—Material Science Division, Lawrence Berkeley National Laboratory, Berkeley, CA 94720, USA. 4.—e-mail: peterh@berkeley.edu

Composites formed by SiC fiber reinforcement of a SiC matrix are materials of interest for use in high temperature, high strength, and high irradiation condition applications. These materials have been considered for use in both fusion and fission reactors due to their excellent physical and neutronic properties. Recent attention has focused on such materials' ability to act as accident-tolerant fuel cladding in light water reactors. The work presented herein studies the swelling behavior of these materials using a novel rapid helium-ion implantation approach. Localized helium implantation was conducted to a dose of $5\times 10^{17}~\rm ions/cm^2$ in fibers and matrix independently. The results showed that the height increase measured using atom force microscopy (AFM) was significantly less for the fibers than the matrix, potentially due to their finer microstructure.

INTRODUCTION

The next generation of nuclear reactors and plasma-facing components (PFCs) for fusion reactors require structural materials that can withstand the harsh operating environments. Hydrogen isotopes combine to form helium while emitting neutrons, inducing irradiation degradation of surfaces of materials exposed to plasma in fusion reactors. 1-In addition, n–α nuclear reactions can cause generation of helium within a large range of materials. 1,3 Irradiation of materials generally increases their hardness and decreases their fracture toughness. Helium (He) specifically leads to formation of He clusters and He-filled cavities (bubbles) within the material, subsequently leading to volumetric swelling, changes in mechanical, magnetic, or electronic properties, blistering, and cracking that result in material failure. Formation of bubbles in copper by 60-keV He-ion irradiation at a temperature of 20°C was reported by Nelson early on, ⁶ followed by similar studies in other materials. ^{2-4,7-9} It was found that the critical dose for the onset of blistering temperature $(6 \pm 1) \times 10^{17} \text{ ions/cm}^2$ for Cu, Mo, and W at dose rates of $10^{15} \text{ ions/cm}^2$ -s to $10^{16} \text{ ions/cm}^2$ -s. $^{9-11}$ The maximum diameter of the blisters was 1 μ m to 2 μ m, with the blisters' size increasing linearly with the implantation energy.

Previous work on this topic is extensive and continues today but has been proven to be time consuming due to the fact that the materials in question must be implanted in a large implanter or accelerator with subsequent detailed TEM and indentation work performed where the large samples are irradiated. The invention of the helium ionbeam microscope (HIM) now allows nanometersized helium implantations at specific regions of interest, while one can observe the formation of blisters and other dose effects in situ. 12 Several doses can be implanted in materials in one session in short periods of time, even within the same grain, since the device allows high-precision implantation. Previous studies have shown that the HIM can be used for helium implantation and leads to a rapid high-throughput experimental approach enables fundamental understanding of He implantation in various materials. 11-14 Various techniques, such as postimplantation atomic force microscopy (AFM), transmission electron microscopy (TEM), scanning electron microscopy (SEM), and nanoindentation, have been used previously to correlate

the swelling induced by 25-keV He irradiation and their dose. $^{11,15-17}$ It has been found that He doses ranging from $1\times10^{17}\,\mathrm{ions/cm^2}$ to $1\times10^{18}\,\mathrm{ions/cm^2}$ can also form He superlattices in bulk material at the temperature and dose conditions expected in some fusion reactor materials. 18,19

Use of SiC fiber/SiC matrix (SiC_f/SiC_m) material has been considered for numerous nuclear applications. $^{20-24}$ Its high strength at high temperatures and low neutron cross-section coupled with a moderate interaction with water or steam make it a good candidate for accident-tolerant fuel for light water reactors. $^{3,20-24}$ Furthermore, its physical properties lead to its consideration as first wall material for fusion reactors. 3,22

In this work, He-ion implantation in SiC_f/SiC_m composite was studied by AFM. The goal of the study is to evaluate experimentally how He implantation affects the swelling as a function of the helium ion dose in the fibers and matrix separately.

EXPERIMENTAL PROCEDURES

Due to its relevance to fusion and fission reactors, $\mathrm{SiC_f/SiC_m}$ composite material was selected for this study. This developmental composite material was acquired from General Atomics, which produces the matrix of the composite using chemical vapor infiltration (CVI) with a two-dimensional (2D) woven fiber structure. The fibers used in the composite were SA3 fibers, the same material as discussed in Refs. ^{24,25}. The $\mathrm{SiC_m}$ was grown via CVI, while the $\mathrm{SiC_f}$ is a SA3 fiber containing both graphite and SiC as a nanocomposite, as revealed by previous characterization of this material. ^{24,25} The nanocrystalline grain structure and residual graphite in SA3 fibers are known from literature. ²⁶

Rectangular samples of each material with dimensions of $10 \text{ mm} \times 10 \text{ mm} \times 2 \text{ mm}$ were used in the tests. The samples were polished using SiC papers and 0.02- μ m colloidal silica solution in a VibroMetTM vibratory polisher machine to roughness of less than 10 nm. The surface roughness was quantified via atomic force microscopy (AFM) using a Nanoscope IIIa prior to He implantation.

He-ion implantation was performed using a lesser known technique via a HIM. The ORION HIM allows precise implantation using a rastered helium ion beam of < 1 nm in size. ¹² This technique allows for novel rapid-throughput testing by implanting small regions with different doses on the exact same

material in the same session, thereby mitigating challenges in previous implantation experiments and accelerating research. Previously, ion-beam implantations were performed using broad ion beams on relatively large, macroscale samples, unless masking techniques were deployed. While large samples can be created in this fashion, such methods face difficulties when comparing unirradiated and irradiated materials at different doses, since seldom the exact same material and sample can be used for comparison at different doses. Only a lengthy process of iterating the sample between testing and implantation multiple times permits study of the effects of different doses on the same sample. This process can be risky since sample damage or loss may occur in between different irradiation steps and instrument schedules. Furthermore, many ion beam accelerators have a near-Gaussian ion-beam current distribution, leading to different beam conditions in each implantation step. Deploying the ORION nanofab for the purpose of He-ion implantation leads to accelerated data acquisition over a wide dose range, with the limitation of low-energy ions and small areas but the benefit that numerous doses can be examined on the same sample and in some cases on the same area of interest. In these experiments, the ability to accurately locate the implantation field was beneficial as it enabled comparison of the effects of He implantation on the matrix and fiber independently in one session. Figure 1 illustrates the workflow of the different He implantation steps using different methods, excluding masking of samples.

In this set of experiments, the gallium-ion beam of the ORION HIM was first used to mill trenches that served as visual markers so that the implanted areas could be located easily for subsequent characterization of the sample by AFM.

Afterwards, the He⁺ beam of the ORION HIM was used to implant 25-keV He ions at a temperature of 20°C into each sample at doses ranging from 5×10^{16} ions/cm² to 5×10^{17} ions/cm² (Fig. 2), at a constant dose rate of $(8.7\pm1)\times 10^{14}$ ions/s-cm². These doses were chosen as they are an order of magnitude above the threshold dose for formation of helium bubbles.²⁷ To vary the dose applied in each implantation, the beam current was maintained at ~ 110 pA while the duration of implantation was varied. All implantations were carried out at room temperature because the ORION nanofab at UC

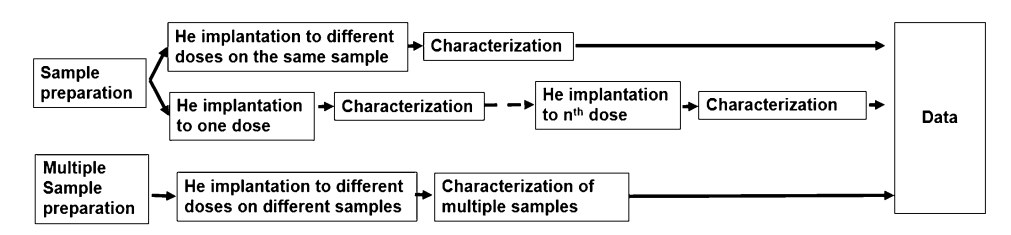


Fig. 1. Characterization of different workflows leading to data generation of helium-ion implanted samples.

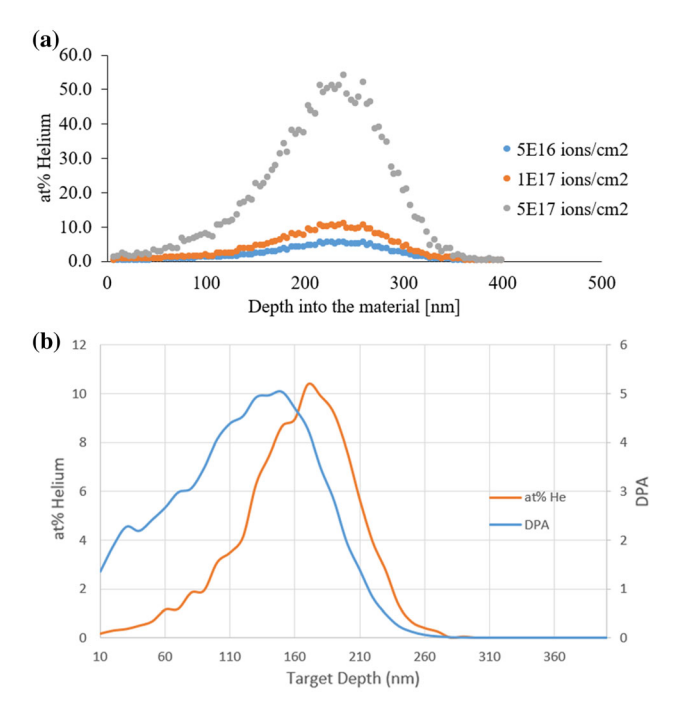


Fig. 2. (a) Helium content as function of depth for the different doses used in this work. (b) Damage profile and He distribution for 10¹⁷ ions/cm².

Berkeley's center for Quantitative Bio Science currently has no heating stage. The different doses in the implantations are displayed in Fig. 2, as calculated using SRIM with displacement threshold energy of 28 eV for carbon and 15 eV for silicon.

After implantation, the samples and the implanted regions were investigated by AFM (Nanoscope IIIa) to assess how the He implantation affected the surface of the samples and the amount of volumetric swelling.

RESULTS AND DISCUSSION

Figure 3 shows a three-dimensional (3D) view of a $20 \ \mu m \times 20 \ \mu m$ He-implanted field on SiC_f/SiC_m composite material. The implantation field was located on a cross-section of the sample so that both fiber and matrix were exposed to the ion beam at the same time. Several features can be observed from this image. The entire implanted area rose above the unimplanted surface. Step height measurements revealed a step height of 18 mm to 22 nm for the matrix and fiber material compared with the unirradiated area. Furthermore, the fibers themselves contained a dimple in the middle before and after irradiation, while the dimple depth was 35 nm to 45 nm on the unimplanted region but ~ 70 nm in the implanted region. However, such views of the sample do not allow direct absolute measurements of the swelling in relation to each other. Previous work found similar dimples in SiC fibers due to the fact that the center of the fiber contains a higher

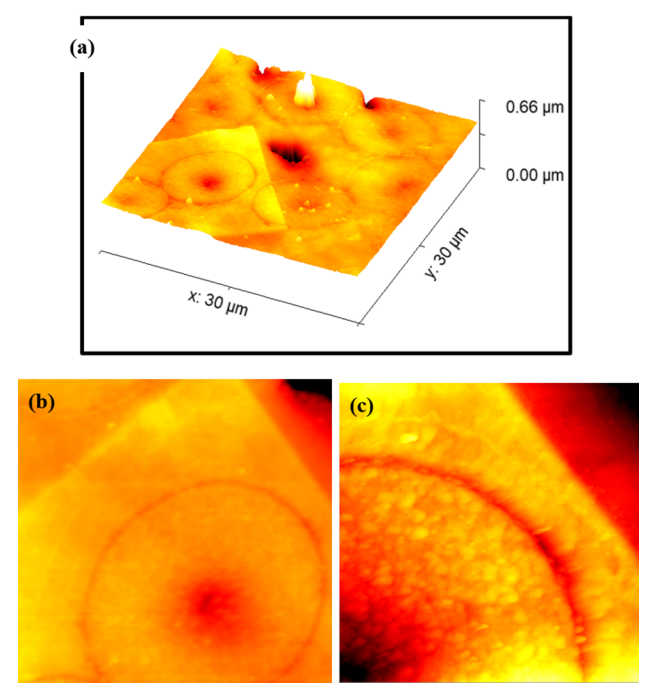


Fig. 3. (a) 3D image of 30 μ m \times 30 μ m scan of implanted area. (b) 2D image of the fiber visible in figure (a) on a 12 μ m \times 12 μ m scale with z-scale of 300 nm; faint rings around the fiber can be seen and are marked in image (c), which shows a 2D image of a 5 μ m \times 5 μ m scan of the same fiber with z-scale of 100 nm.

concentration of carbon nanograins in between the nanograined SiC grains and polishing removes the softer area preferentially. ^{24–26}

Furthermore, Fig. 3b shows that rings around the fiber are visible by AFM, as previously reported using SEM and SEM-STEM.²⁵

Whenever performing AFM measurements, great attention must be given to surface finish and surface preparation. Root-mean-square (RMS) measurements showed that the RMS surface roughness changed insignificantly after ion-beam irradiation, from 6.4 nm in the unirradiated SiC matrix to 7.2 nm in the irradiated area. Such a minimal change in the surface roughness of SiC after He implantation has been seen in other studies.²⁸

Further dose-dependent He-ion beam irradiations were carried out on the material's cross-section, where the fibers are exposed lengthwise to the ion beam; in this way, direct comparisons can be made. Figure 4 illustrates this series of experiments where SiC fibers embedded in the SiC matrix were subjected to implantation from $5 \times 10^{16} \text{ ions/cm}^2$ to $5 \times$ 10¹⁷ ions/cm². It can be seen that the implanted $10 \ \mu m \times 10 \ \mu m$ square implants rose above the surrounding surface due to the implantation. All images are plotted on the same height scale of 200 nm, so it is obvious that higher doses led to stronger height increases. In addition, the plots use the same scale as well to allow direct comparison between the different doses. The plots on the side of the AFM scans are line scans across the length axis of the implanted

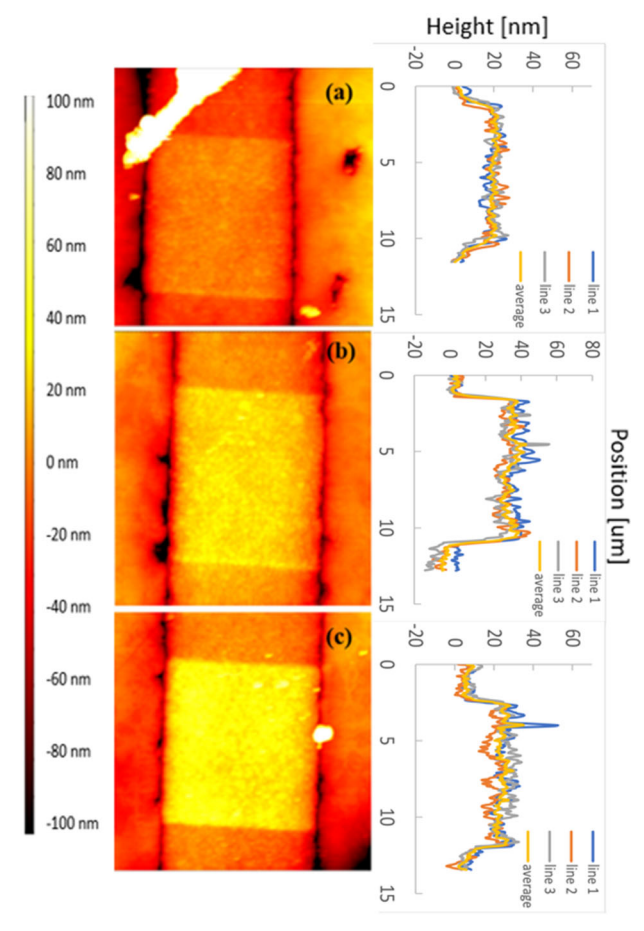


Fig. 4. AFM scans of fibers implanted to different doses and associated cross-section line scans. Three line scans at different locations and the average are displayed: (a) 5×10^{16} ions/cm², (b) 1×10^{17} ions/cm², and (c) 5×10^{17} ions/cm².

material, enabling comparison of the height increase from the original fiber axis on the same scale. The fibers selected for analysis were those with widths approximately equal to the diameter of the fiber, thus one can assume that the cross-section was performed through the middle of the fiber. Interestingly, despite the higher carbon content in the middle of the fiber as reported in literature, ^{24–26} no difference in swelling was found across the fiber width.

A similar analysis was performed on the matrix component of the composite. The same three doses of $5\times 10^{16}~\rm ions/cm^2$, $1\times 10^{17}~\rm ions/cm^2$ and $5\times 10^{17}~\rm ions/cm^2$ were implanted in $10~\mu m\times 10~\mu m$ fields onto the material. The associated AFM images are shown in Fig. 5 with the line scans. Since the entire surrounding material is matrix material, it is expected and found that the line scans can be performed in any direction, in contrast to the fiber swelling measurements described above. It can also be seen that the swelling increases with dose in this case. All figures are shown at the same height scale of 175 nm.

Figure 6 compares the average effect of helium dose on the fiber versus the matrix, revealing that the fiber swells significantly less (by nearly a factor

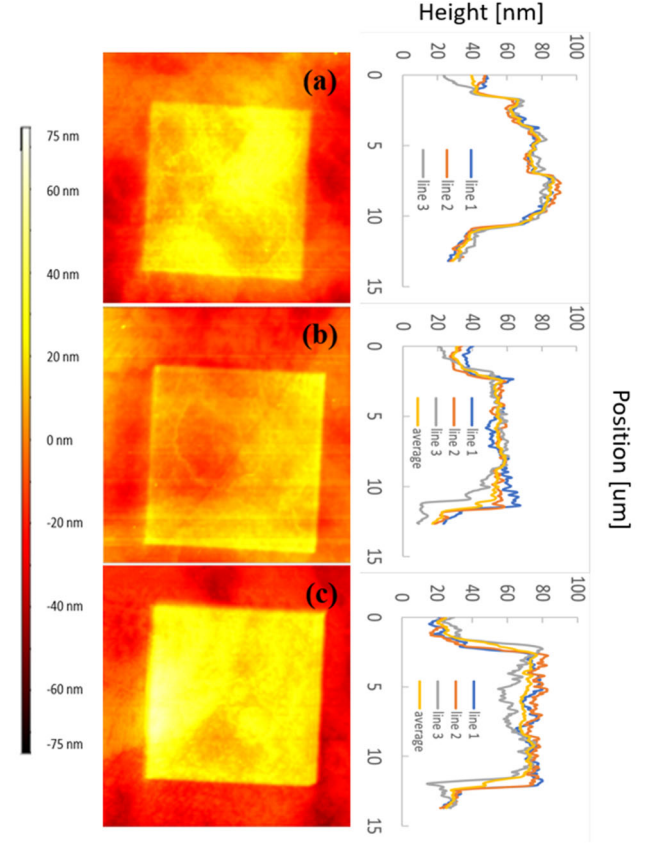
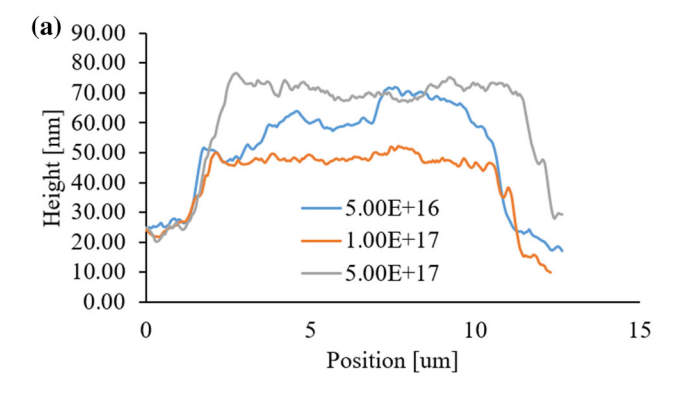


Fig. 5. AFM scans of SiC_m implanted to different doses and associated cross-section line scans. Three line scans at different locations and the average are displayed: (a) 5 \times 10 16 ions/cm², (b) 1 \times 10 17 ions/cm², and (c) 5 \times 10 17 ions/cm².

of two) in comparison with the matrix. At the highest dose (5 \times 10¹⁷ ions/cm²), the fiber swells by only 30 nm while the matrix swells by 50 nm. A dose versus height increase plot is shown in Fig. 5c. One may speculate about this observation, and two potential explanations can be considered: First, the SiC matrix material is a fully dense material at this length scale. Numerous previous publications have clearly shown that the grains range from 100 nm to micrometers in size, depending on the region one looks at, with no pores between grains. The fibers, however, show size of 100 nm to 200 nm, with graphite in between, as previously reported.²⁴⁻²⁶ One may argue that this smaller grain structure of the fibers enables accommodation of significantly more helium in contrast to the larger matrix grains due to the higher density of grain boundaries. The second explanation is that a fiber containing more carbon has a lower density, thus the ion beam can penetrate deeper into the material, distributing the same amount of helium through a deeper depth and thereby reducing the real density of helium, with bubbles staying in the nucleation than growth phase, leading to less swelling. However, even large amounts of carbon will not be able to change the depth significantly enough to cause this potential phenomenon. The reader is reminded that this work



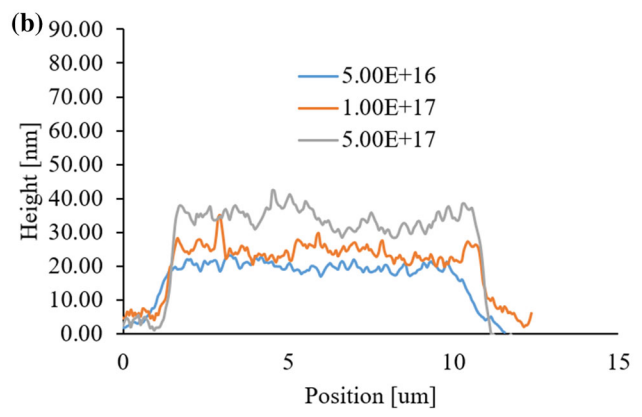


Fig. 6. Average line scans of (a) matrix and (b) fiber material at three different doses. It is obvious that the matrix material swells more in response to helium implantation.

features helium-induced swelling only, and not the classical neutron-induced swelling that is primarily based on displacement damage; the arguments made here are solely focused on helium accommodation within the material. Most data in the literature come from heavy-ion beam and neutron irradiation studies. $^{29-34}$ Although several studies on helium implantation in SiC have been carried out, 35-38 not all were performed at room temperature and on the same polymorphs, and they do not evaluate the swelling by AFM, making comparisons with literature difficult. However, Leclerc et al. studied swelling of SiC using 50-keV He ions in a similar dose range $(1 \times 10^{16} \text{ ions/cm}^2)$ to $1 \times 10^{17} \text{ ions/cm}^2$. In that study, single crystals of SiC with hexagonal crystal structure (4H-SiC) showed a step height of $50 \pm 10 \text{ nm}$ for $5 \times 10^{16} \text{ ions/cm}^2$ and $60 \pm 10 \text{ nm}$ for $1 \times 10^{17} \text{ ions/cm}^2$. In the present study, however, the matrix material swelled by $\sim 30 \text{ nm}$ for $5 \times 10^{16} \text{ ions/cm}^2$ $1 \times 10^{17} \text{ ions/cm}^2$. and by $\sim 38 \text{ nm}$ for This discrepancy explained by several phenomenon: Firstly, in this study, 25-keV He implantation was used, thus the penetration depth is less, leading to less volume affected and therefore less swelling. In addition, the CVI SiC_m in the composites used in this study has a cubic (β -SiC) crystal structure, which could show different behavior under helium implantation.

Using the same technique as described here, chemical vapor deposition (CVD) SiC was implanted with doses from $1\times 10^{16}~\rm ions/cm^2$ to $1\times 10^{18}~\rm ions/cm^2$. While the step was not measured, it was observed that the implantation fields did swell and that the SiC was amorphized at a dose of $1\times 10^{17}~\rm ions/cm^2$. Such amorphization of SiC was observed at doses of $1\times 10^{17}~\rm ions/cm^2$ and greater. There is a large amount of work showing that ion-beam irradiations will amorphize SiC, which will decrease the density and cause some increase in swelling. He is therefore expected that, at the higher doses, the amorphization would contribute to the swelling of the SiC. However, the amount of swelling from amorphization is expected to be minimal.

The first wall in a nuclear fusion device will experience a tremendous amount of helium impacts. Therefore, one may conclude that, based on swelling considerations, the nonstoichiometric SiC fibers would behave better than the CVI-produced matrix. Of course, this comparison does not consider sputtering and erosion issues, or displacement damage, which are different issues in an actual application. One may speculate whether a nanosized SiC material without graphite would behave optimally, combining both $_{
m the}$ fine microstructure stoichiometry. In addition, the difference in swelling between the fibers and matrix could affect the overall behavior of the composite, as it is governed by the interplay between the fibers and matrix. Their different behaviors would cause a change in this interplay that would affect the overall behavior of the composite. The ability to independently sample the effects of He implantation on different phases in a material or components in a composite will allow for better modeling and deeper understanding of the overall behavior.

CONCLUSION

- 1. A rapid-throughput helium implantation method using the ORION Nanofab HIM, in combination with AFM, is introduced to study ${\rm SiC_{f}/SiC_{m}}$ composites.
- The highly localized method employed here enables separate study of the behavior of the fibers versus the matrix without the need for masks.
- 3. It is found that the SiC fibers swell significantly less than the CVI-produced SiC matrix when considering doses as high as 5×10^{17} ions/cm².

ACKNOWLEDGEMENTS

The authors would like to thank Dr. Frances Allen for assistance with ORION HIM operation. Support was provided by NSF-DMR Program # 1807822. Further, the authors want to thank Gen-

eral Atomics for providing the sample material for this research.

REFERENCES

- L.K. Mansur, E.H. Lee, P.J. Maziasz, and A.P. Rowcliffe, J. Nucl. Mater. 141-143, 633 (1986).
- F.C. Wu, Y.B. Zhu, Q. Wu, X.Z. Li, P. Wang, and H.A. Wu, J. Nucl. Mater. 496, 265 (2017).
- L.L. Snead, R.H. Jones, A. Kohyama, and P. Fenici, J. Nucl. Mater. 233-237, 26 (1996).
- S. Saremi, R. Xu, F.I. Allen, J. Maher, J.C. Agar, R. Gao, P. Hosemann, and L.W. Martin, Phys. Rev. Mater. 2, 084414
- R.E. Stoller and D.M. Stewart, J. Nucl. Mater. 417, 1106 (2011).
- R.S. Nelson, Philos. Mag. (1798-1977) 9, 343 (1964).
- W. Bauer and G.J. Thomas, J. Nucl. Mater. 42, 96 (1972).
- B.B. Cipiti and G.L. Kulcinski, J. Nucl. Mater. 347, 298
- S.K. Erents and G.M. McCracken, Radiat. Eff. 18, 191
- 10. F. Allen, P. Hosemann, and M. Balooch, U.C. Berkeley, Berkeley, California, arXiv:1909.02133 (2019).
- Y. Yang, D. Frazer, M. Balooch, and P. Hosemann, J. Nucl. Mater. 512, 137 (2018).
- V. Veligura, G. Hlawacek, R.P. Berkelaar, R. van Gastel. H.J.W. Zandvliet, and B. Poelsema, Beilstein J. Nanotechnol. 4, 453 (2013).
- G. Hlawacek, V. Veligura, R. van Gastel, and B. Poelsema, J. Vac. Sci. Technol. B 32, 020801 (2014).
- F. Bergner, G. Hlawacek, and C. Heintze, J. Nucl. Mater. 505, 267 (2018).
- Z.J. Wang, F. Allen, Z.-W. Shan, and P. Hosemann, Acta Mater. 121, 78 (2016).
- P.B. Johnson, R.W. Thomson, and K. Reader, J. Nucl. Mater. 273, 117 (1999).
- D. Frazer, J. Szornel, D.L. Krumwiede, K.A. Terrani, and P. Hosemann, Exp. Mech. 57, 1081 (2017).
- P.B. Johnson and D.J. Mazey, Nature 281, 359 (1979). 18.
- R.W. Harrison, G. Greaves, J.A. Hinks, and S.E. Donnelly, Sci. Rep. 7, 7724 (2017).
- P. Hosemann, D. Frazer, M.F. Ashby, and M. Fratoni, Scr. Mater. 143, 181 (2018).
- K. Yueh and K.A. Terrani, J. Nucl. Mater. 448, 380
- L.L. Snead, T. Nozawa, M. Ferraris, Y. Katocm, R. Shinavski, and M. Sawan, J. Nucl. Mater. 417, 330 (2011).

- C.P. Deck, G.M. Jacobsen, J. Sheeder, O. Gutierrez, J. Zhang, J. Stone, H.E. Khalifa, and C.A. Back, J. Nucl. Mater. 466, 667 (2015).
- 24. D. Frazer, M.D. Abad, D. Krumwiede, C.A. Back, H.E. Khalifa, C.P. Deck, and P. Hosemann, Compos. Part A 70, 93 (2015).
- J. Kabel, M. Balooch, D. Frazer, C. Deck, T. Koyanagi, K. Terrani, and P. Hosemann, Int. Congr. Adv. Nucl. Power Plants, 911 (2016).
- Y. Katoh, K. Ozawa, C. Shih, T. Nozawa, R.J. Shinavski, A. Hasegawa, and L.L. Snead, J. Nucl. Mater. 448, 448 (2014). C.H. Zhang, S.E. Donnelly, V.M. Vishnyakov, and J.H.
- Evans, J. Appl. Phys. 94, 6017 (2003).
- G. Hong-Yan, G. Chang-Chun, X. Min, G. Li-Ping, C. Ji-Hong, and Y. Qing-Zhi, *Chin. Phys. B* 24, 3 (2015). M.I. Idris, H. Konishi, M. Imai, K. Yoshida, and T. Yano,
- Energy Procedia 71, 328-336 (2015).
- L.L. Snead and J.C. Hay, J. Nucl. Mater. 273, 213 (1999).
- A.L. Ryazanov, A.V. Klaptsov, A. Kohyama, and H. Kishimoto, J. Nucl. Mater. 301-311, 1107 (2002).
- V. Heera, J. Stoemenos, R. Kogler, and W. Skorupa, J. Appl. Phys. 77, 2999 (1995).
- W.J. Weber, L.M. Wang, N. Yu, and N.J. Hess, Mater. Sci. Eng. A 253, 62 (1998).
- S.M. Tunhuma, M. Diale, J.M. Nel, M.J. Madito, T.T. Hlatshwayo, and F.D. Auret, Nucl. Instrum. Methods Phys. Res., Sect. B (2018).
- Y. Yang, C. Zhang, C. Su, Z. Ding, and Y. Song, Nucl. Instrum. Methods Phys. Res. Sect. B 449, 54 (2019).
- J.F. Barbot, M.F. Beaufort, M. Texier, and C. Tromas, J. Nucl. Mater. 413, 162 (2011).
- C. Tromas, V. Audurier, S. Leclerc, M.F. Beaufort, A. Declemy, and J.F. Barbot, J. Nucl. Mater. 373, 142 (2008).
- B.S. Li, C.H. Zhang, H.H. Zhang, T. Shibayama, and Y.T. Yang, Vacuum 86, 452 (2011).
- S. Leclerc, A. Declémy, M.F. Beaufort, C. Tromas, and J.F. Barbot, J. Appl. Phys. 98, 113506 (2005).
- L.L. Snead, S.J. Zinkle, J.C. Haym, and M.C. Osborne, Nucl. Instrum. Methods Phys. Res. Sect. B 141, 123 (1998).
- A. Debelle, A. Boulle, A. Chartier, F. Gao, and W.J. Weber, Phys. Rev. B Condens. Matter Mater. Phys. 90, 174112 (2014).
- J.M. Williams, C.J. McHargue, and B.R. Appleton, Nucl. Instrum. Methods Phys. Res. 209-210, 317 (1983).

Publisher's Note Springer Nature remains neutral with regard to jurisdictional claims in published maps and institutional affiliations.